FULL PAPER

Dalton
www.rsc.org/dalton

Novel Au(III) complexes of aminoquinoline derivatives: crystal structure, DNA binding and cytotoxicity against melanoma and lung tumour cells †

Ting Yang,[a] Chao Tu,[a] Junyong Zhang,[a] Liping Lin,[b] Xianming Zhang,[c] Qin Liu,[a] Jian Ding,[b] Qiang Xu[c] and Zijian Guo*[a]

[a] *State Key Laboratory of Coordination Chemistry, Coordination Chemistry Institute, Nanjing University, Nanjing 210093, P. R. China. E-mail: zguo@netra.nju.edu.cn.*

[b] *Division of Anti-tumor Pharmacology, State Key Laboratory for New Drug Research, Shanghai Institute of Materia Medica, Shanghai Institute of Biological Sciences, Shanghai 200031, P. R. China*

[c] *State Key Laboratory of Pharmaceutical Biotechnology, Nanjing University, Nanjing 210093, P. R China*

Received 7th May 2003, Accepted 8th July 2003
First published as an Advance Article on the web 28th July 2003

Three novel gold(III) complexes [Au(Quinpy)Cl]Cl (**1**), [Au(Quingly)Cl]Cl (**2**) and [Au(Quinala)Cl]Cl (**3**) [*N*-(8-quinolyl)pyridine-2-carboxamide = HQuinpy; *N*-(8-quinolyl)glycine-carboxamide = HQuingly; *N*-(8-quinolyl)-L-alanine-carboxamide = HQuinala] have been synthesized and characterized. The crystal structures of complexes **2** and **3** reveal that Au(III) is coordinated by three N atoms from the ligand and one Cl^- anion. Complex **2** crystallized in the monoclinic system while complex **3** crystallized in the orthorhombic system. The complexes were tested against a series of tumour cell lines including B16-BL6, P388, HL-60, A-549 and BEL-7402. The data show that complex **1** is highly cytotoxic against the A-549 cells with an inhibition rate of 94.4% at a concentration of 10^{-6} mol L^{-1}. Complex **3** is active against B16-BL6 with an inhibition rate of 67.52% at a concentration of 10^{-7} mol L^{-1}. The interactions of complexes **1**–**3** with calf thymus (CT) DNA and 5′-GMP were investigated by UV-vis, fluorescence and ESMS spectroscopies. The data show that the interaction between Au(III) complexes and CT-DNA may be the intercalation effect, and complex **3** forms a 5′-GMP adduct as detected by ESMS.

Introduction

The clinical success of cisplatin for the treatment of a variety of cancer diseases has promoted extensive studies on the application of metals in medicine.[1–4] Gold(III) has a configuration isoelectronic with Pt(II), and therefore was among the first non-Pt metals explored for antitumour potential.[5] Similar to Pt(II) complexes, Au(III) compounds are able to bind to DNA which may account for their cytotoxic activity.[6,7]

One of the key problems that hampered the development of Au(III) complexes is their low stability under physiological conditions.[8,9] Gold(III) compounds are highly oxidative and are able to oxidize a series of biomolecules such as methionine[10] and glycine.[11] The stability of Au(III) compounds can be enhanced by introducing chelating ligands, examples include [Au(cyclam)]-$(ClO_4)_2Cl$,[12] $[AuCl_2(esal)]$ (esal, ethylsalicyladiminate),[13] $[Au(phen)Cl_2]Cl$,[14] $[Au(Mephpy)Cl_2]$ (Mephpy = *N*-(4-methylphenyl)-2-pyridine carboxamide),[15] $[Au(bipy)(OH)_2](PF_6)$[16] and $[Au(bipy^c\text{-}H)(OH)](PF_6)$ ($bipy^c$-H = 6-(1,1-dimethylbenzyl)-2,2′-bipyridine).[16] In these complexes, Au(III) is coordinated by at least two chelating nitrogen donors which lowers the redox potential of the metal center and thereby stabilizes the complexes.

In this work, we have synthesized and characterized three new gold(III) compounds, *i.e.*, [Au(Quinpy)Cl]Cl (**1**); [Au(Quingly)-Cl]Cl (**2**); [Au(Quinala)Cl]Cl (**3**) (Chart 1). The latter two complexes were structurally characterized by X-ray diffraction. All the ligands coordinate to Au(III) in a tridentate mode forming two five-membered chelate rings.

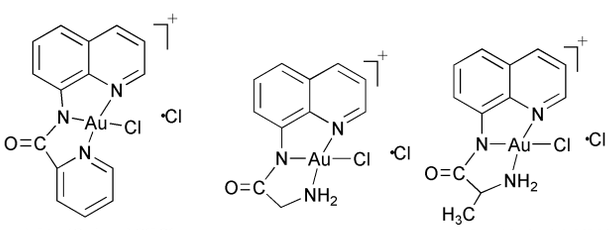

Chart 1 Schematic drawing of the three new gold(III) complexes.

Experimental

Materials and methods

Solvents such as methanol, acetonitrile, nitromethane and DMSO were all analytical reagents and used as received. Hydrogen tetrachloroaurate(III) hydrate was purchased from Shanghai Chemical Reagent Co. Ltd. The disodium salt of 5′-GMP and the calf thymus DNA were purchased from Sigma.

Three ligands *N*-(8-quinolyl)pyridine-2-carboxamide (HQuinpy, HL^1); *N*-(8-quinolyl)glycine-carboxamide (HQuingly, HL^2); *N*-(8-quinolyl)-L-alanine-carboxamide (HQuinala, HL^3) were prepared following the reported procedures.[17,18]

The infrared spectra were recorded on a Bruker VECTOR22 spectrometer as KBr pellets (4000–500 cm^{-1}), and elementary analysis was performed on a Perkin-Elmer 240c analytical instrument. NMR data were acquired on a 500 MHz Bruker DMX spectrometer (^1H 500 MHz) using standard pulse sequences. Electrospray mass spectra were recorded using an LCQ electron spray mass spectrometer (ESMS, Finnigan) and the predicted isotope distribution patterns for each of the complexes were calculated using the Isopro 3.0 program.[19]

† Electronic supplementary information (ESI) available: UV spectra of **3**, **3** + NaCl, and **1** + calf thymus DNA; fluorescence spectra of the CT-DNA-EB system with increasing amounts of **1** or **3**. See http://www.rsc.org/suppdata/dt/b3/b305109a/

DOI: 10.1039/b305109a

Table 1 Crystal data and structure refinement for complexes **2** and **3**

	2	**3**
Empirical formula	$C_{11}H_{10}N_3O_1AuCl_2$	$C_{12}H_{12}N_3O_1AuCl_2$
Formula weight	468.09	482.11
T/K	293(2)	293(2)
Crystal system	Monoclinic	Orthohombic
Space group	$P2_1/c$	$P2_12_12_1$
a/Å	6.5239(9)	6.6540(10)
b/Å	19.001(3)	9.262(2)
c/Å	10.1653(14)	22.169(4)
β/°	90.855(3)	
V/Å^3	1260.0(3)	1366.3(4)
Z	4	4
μ/mm^{-1}	12.089	11.152
Reflections collected	7202	1419
Independent reflections	2735 (R_{int} = 0.0731)	1419 (R_{int} = 0.0000)
Goodness-of-fit on F^2	0.827	1.153
Final R indices [$I>2\sigma(I)$]	$R1$ = 0.0371, $wR2$ = 0.0711	$R1$ = 0.0666, $wR2$ = 0.2143
Largest difference peak, hole/e Å^{-3}	1.711, −1.138	2.635, −2.915

UV-vis spectra were recorded on a UV-3100 spectrometer. Fluorescence spectra were recorded on an AMINCO Bowman Series 2 Luminescence Spectrometer.

Preparations

Preparations of the complexes. The complexes **1**–**3** were prepared as follows. $HAuCl_4$ (0.1 mmol, 41 mg) and ligand HL[1] (0.1 mmol, 25 mg) were separately dissolved in 2 ml of methanol, then mixed in a 1 : 1 molar ratio. The mixture was refluxed for 4 h. A brown precipitate formed when the solution was cooled to room temperature, which was then collected by filtration. The brown solid was recrystallized from nitromethane, giving rise to [AuL[1]Cl]Cl (**1**). Complexes **2** and **3** were prepared similarly, and recrystallized from acetonitrile by slow evaporation. Crystals of complexes **2** and **3** were suitable for X-ray determination.

Elemental Anal. Found (calculated) for complex **1** (%): C, 23.3 (23.5); H, 1.94 (1.90); N, 8.14 (8.18). ^{1}H NMR of complex **1** in D_6-DMSO (ppm): 9.376 (d, 1H), 9.224 (d, 1H), 9.114 (d, 1H), 8.690 (m, 2H), 8.245 (d, 1H), 8.162 (t, 1H), 8.130 (t, 1H), 8.032 (d, 1H), 7.926 (t, 1H). IR of complex **1** (cm^{-1}): $\nu_{C=O}$: 1679.6, $\nu_{C=C}$: 1604.30, $\nu_{C=N}$: 1541.8. Elemental Anal. Found (calculated) for complex **2** (%): C, 28.2 (28.6); H, 2.14 (2.16); N, 8.97 (8.92). ^{1}H NMR of complex **2** in D_6-DMSO (ppm): 9.196 (d, 1H), 9.070 (d, 1H), 8.533 (d, 1H), 8.055 (m, 1H), 7.895 (d, 1H), 7.826 (t, 1H), 4.269 (s, 2H). IR of complex **2** (cm^{-1}): ν_{N-H}: 3447.8, $\nu_{C=O}$: 1658.0, $\nu_{C=N}$: 1561.1. Elemental Anal. Found (calculated) for complex **3** (%): C, 30.0 (30.3); H, 2.49 (2.47); N, 8.71 (8.68). ^{1}H NMR of complex **3** in D_6-DMSO (ppm): 9.912 (d, 1H), 9.076 (d, 1H), 8.568 (d, 1H), 8.079 (m, 1H), 7.904 (d, 1H), 7.827 (t, 1H), 4.471 (s, 1H), 1.51(s, 3H). IR of complex **3** (cm^{-1}): ν_{N-H}: 3447.2, $\nu_{C=O}$: 1664.9, $\nu_{C=C}$: 1592.5.

All three compounds are fairly soluble and stable in organic solvents such as methanol, acetonitrile, DMF and DMSO, but poorly soluble in water.

Reaction of the complexes with 5′-GMP and DNA. Au(III) complex **1** (**2** or **3**) (0.05 mmol) was dissolved in methanol, and an aqueous solution of 5′-GMP (0.05 mmol) was added with stirring at room temperature. After 48 h reaction, the solution was recorded by ESMS.

Complex **1** (**2** or **3**) was dissolved in a mixed solution of 50% DMSO and 50% H_2O giving rise to a solution of 0.2 mM. The solutions were monitored by UV-vis spectroscopy for 24 h. The solution behaviour of **1** (**2** or **3**) in the presence of Cl^- (50 mM) was also followed by UV for 24 h.

The DNA concentrations were determined by measuring the UV absorption at 260 nm and taking the molar absorption coefficient (ε_{260}) of CT-DNA as 6600 mol^{-1} L cm^{-1}. The absorption spectra in the UV-vis region were recorded at room temperature. The gold(III) complexes **1**, **2** and **3** were dissolved in a mixed solvent of 50% DMSO and 50% Tri-HCl buffer (5 mM Tri-HCl, 50 mM NaCl, pH 7.34) at concentrations of 1.9×10^{-4} M, 2.1×10^{-4} M and 2.1×10^{-4} M, respectively. Electronic spectra were recorded before and 1 h, 2 h and 3 h after addition of calf thymus DNA (r = 0.1, concentrations were 1.9×10^{-5} M, 2.1×10^{-5} M and 2.1×10^{-5} M, respectively).

The fluorescence spectra were recorded at room temperature. λ_{ex} was at 526 nm and λ_{em} at 600 nm. The gold(III) complexes **1**, **2** and **3** were dissolved in a mixed solvent of 50% DMSO and 50% Tri-HCl buffer (5 mM Tri-HCl, 50mM NaCl, pH 7.34) at concentrations of 3.5×10^{-4} M, 2.4×10^{-4} M and 3.1×10^{-4} M, respectively. The experiment was carried out by titrating the solution of the gold complexes (20 μL per scan) into samples containing 4.9×10^{-5} M of DNA and 4.9×10^{-5} M EB (ethidium bromide).

Crystallography

Table 1 summarises the crystal data, data collection, structural solution and refinement parameters for complexes **2** and **3**. The orange block crystal of complex **2** of approximate dimensions 0.15 × 0.10 × 0.10 mm was mounted on a Siemens SMART CCD diffractometer. Reflection data were measured at 293 K using graphite-monochromated Mo-Kα (λ = 0.71073 Å) radiation with a detector distance of 4 cm and swing angle of −35°. The program SAINT[20] was used for data reduction and empirical absorption correction was carried out using the SADABS program.[21] The structure was solved by Patterson methods that revealed the position of all non-hydrogen atoms and refined using the full-matrix least-squares method on F^2_{obs} using the SHELXTL software package.[22] All non-hydrogen atoms were placed in calculated positions. The molecular graphics were created using SHELXTL. Atomic scattering factors and anomalous dispersion corrections were taken from ref. 23.

The crystal of complex **3** was also an orange block that was mounted on a glass fiber and used for data collection. Cell constants and an orientation matrix for data collection were obtained by least-squares refinement of diffraction data from 34 reflections in the range $1.84 < \theta < 24.97$ on a Simens P4 four-circle diffractometer. Data were collected at 293 K using monochromated Mo-Kα radiation and the ω–2θ scan technique with a variable scan speed 5.0–50.0° min^{-1} in ω and corrected for Lorentz and polarization effects. An empirical absorption correction was made (ψ-scan). The structure was solved by Patterson methods and completed by iterative cycles of least-squares refinement and ΔF-syntheses. H-atoms were located in their calculated positions and treated as riding on the atoms to which they are attached. All non-hydrogen atoms

were refined anisotropically except C(2) due to non-positive definition (NPD). All calculations were carried out using the SHELXTL program.[22]

CCDC reference numbers 210004 and 210005.

See http://www.rsc.org/suppdata/dt/b3/b305109a/ for crystallographic data in CIF or other electronic format.

Cytotoxicity assay

Tumour cell lines used in this work were grown in RPMI-1640 medium supplement with 10% (vol/vol) calf serum, 2 mmol L^{-1} glutamine, 100 U mL^{-1} penicillin (U = 1 unit of activity), and 100 μg mL^{-1} streptomycin (GIBCO, Grand Island, NY) at 310 K under 5% CO_2. Cells in 100 μL culture medium were seeded into 96-well plates (Falcon, CA).

For melanoma B16-BL6, murine leukemia P-388 and human leukemia HL-60 cells, the microculture MTT [3-(4,5-dimethyl-2-thiazolyl)-2,5-diphenyl-2*H*-tetrazolium bromide] assay [24] was conducted as follows. The B16-BL6 cells were treated with compounds **2** and **3** in a concentration gradient to give final concentrations at 1×10^{-6}, 1×10^{-7}, 1×10^{-8}, 1×10^{-9} M, respectively. Other cells were treated in triplicate with grade concentrations of complex **1** and the reference drug cisplatin at 310 K for 48 h. A 20 μL aliquot of MTT solution (5 mg mL^{-1}) was added directly to all the appropriate wells. The culture was then incubated for 4 h. A 50 μL aliquot of 50% SDS [$CH_3(CH_2)_{11}OS\ O_3Na$]–5% isobutyl alcohol–0.01 mol mL^{-1} hydrochloride solution was added. After the plates were incubated overnight, the optical densities were read on a plate reader (model VERSA Max, Molecular Devices) at 570 nm.

For human hepatoma BEL-7402 and lung adenocarcinoma A-549 cell, the growth inhibition was analysed by the sulforhodamine B (SRB) assay.[25] Simply, following the treatment with complex **1** for 72 h, the cell cultures were fixed with 10% trichloroacetic acid and incubated for 60 min at 277 K. Then, the plates were washed and dried, SRB solution (0.4% wt/vol in 1% acetic acid) was added and the culture was incubated for an additional 15 min. After the plates were washed and dried, bound stain was solubilized with Tris buffer, and the optical densities were read on the same plate reader at 515 nm. The growth inhibitory rate of treated cells was calculated by $(OD_{control} - OD_{test})/OD_{control} \times 100\%$.

Results and discussion

Crystallography

The molecular structure and numbering scheme for complex **2** is shown in Fig. 1. Selected bond lengths and angles are listed in Table 2. In this molecule, Au(III) adopts a distorted square planar geometry coordinated by three N atoms of the ligand and a chloride anion. The mean deviation from the best AuN_3Cl plane [Au(1), N(1), N(2), N(3), Cl(1)] is 0.0417 Å, and the deviation of the Au atom from this best plane is 0.0373Å. It is notable from Fig. 2 that the AuN_3Cl plane is nearly co-planar with the quinoline ring, and the mean deviation from this large

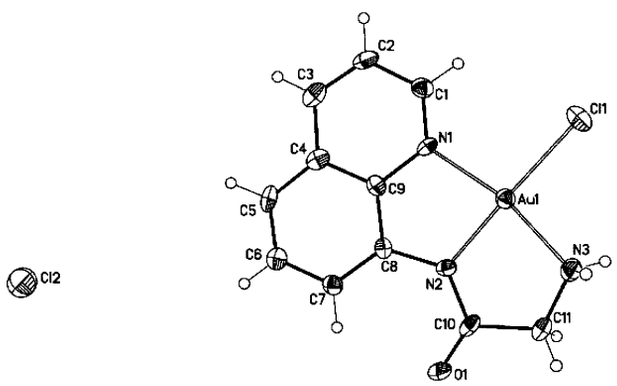

Fig. 1 An ORTEP view of complex **2**.

Table 2 Selected bond lengths (Å) and angles (°) for complex **2**

Au(1)–N(1)	2.027(6)	Au(1)–N(2)	1.953(6)
Au(1)–N(3)	2.024(6)	Au(1)–Cl(1)	2.277(2)
N(1)–C(1)	1.284(9)	N(1)–C(9)	1.393(9)
N(2)–C(8)	1.431(9)	N(2)–C(10)	1.339(9)
N(3)–C(11)	1.466(10)	C(10)–O(1)	1.215(10)
C(8)–C(9)	1.375(10)	C(10)–C(11)	1.527(11)
N(1)–Au(1)–N(2)	83.5(3)	N(2)–Au(1)–N(3)	83.1(3)
N(3)–Au(1)–Cl(1)	94.8(2)	Cl(1)–Au(1)–N(1)	98.6(2)
C(8)–N(2)–C(10)	128.5(7)	O(1)–C(10)–C(11)	121.5(7)
C(8)–N(2)–Au(1)	113.6(5)	C(9)–N(1)–Au(1)	108.8(5)
Au(1)–N(1)–C(1)	128.8(6)	N(2)–C(8)–C(9)	113.2(6)
Au(1)–N(2)–C(10)	118.0(6)	N(2)–C(10)–C(11)	113.0(8)
C(11)–N(3)–Au(1)	109.7(5)		

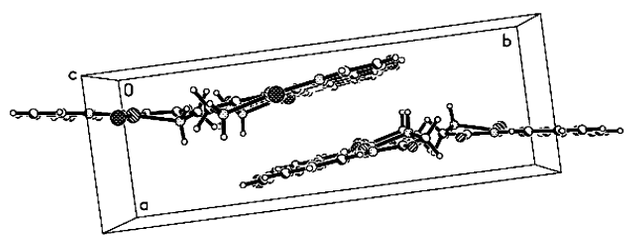

Fig. 2 Structure of complex **2** packed along the *a*-axis.

best plane is 0.0736 Å. In the crystal cell the complex is packed in a head to tail fashion and the distance between the two adjacent planes is 3.1906 Å, which shows a strong π–π interaction between two adjacent molecules. The approximate square-planar coordination of the Au(III) atom generates two five-membered rings. The torsion angles Au(1)–N(2)–C(8)–C(9), Au(1)–N(1)–C(9)–C(8), Au(1)–N(2)–C(10)–C(11), Au(1)–N(3)–C(11)–C(10) are 3.4(7)°, −4.2(8)°, 2.0(9)°, and −18.8(9)° respectively. The shortest Au–N bond is Au(1)–N(2) which is shared by the two five-membered chelate rings. All of the Au–N and Au–Cl bond lengths are in the expected region for Au(III) complexes.[26] The chloride counterion of complex **2** dissociates in the space. Intermolecular hydrogen bonds have been observed, and the D ··· A separations are 2.050 Å, 2.259 Å for N(3) ··· O(1b) and N(3) ··· Cl(2b), respectively (symmetry code: x, $-y + 5/2$, $z + 1/2$ and $-x + 2$, $-y + 2$, $-z + 1$). The D–H ··· A angles are *ca.* 136.77° and 159.28° for N(3)–H(3B) ··· O(1) and N(3)–H(3C) ··· Cl(2), respectively.

The crystal structure of complex **3** is shown in Fig. 3. Selected bond lengths and angles are listed in Table 3. Similar to complex **2**, the Au(III) in complex **3** is also coordinated in a slightly distorted square planar geometry composed of three nitrogen atoms and one chloride anion. The mean deviation from the best plane AuN_3Cl [Au(1),N(1),N(2),N(3),Cl(1)] is 0.0365 Å. Similar to complex **2**, the AuN_3Cl plane is nearly co-planar with the quinoline ring (Fig. 4) with a mean deviation from this large

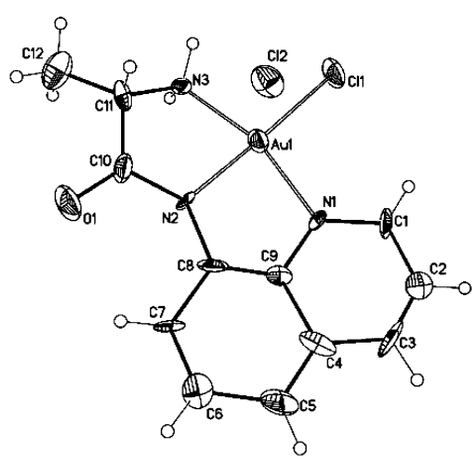

Fig. 3 An ORTEP view of complex **3**.

Table 3 Selected bond lengths (Å) and angles (°) for complex **3**

Au(1)–N(1)	2.02(3)	Au(1)–N(2)	1.98(3)
Au(1)–N(3)	1.98(3)	Au(1)–Cl(1)	2.278(10)
N(1)–C(1)	1.39(5)	N(1)–C(9)	1.38(5)
N(2)–C(8)	1.40(4)	N(2)–C(10)	1.39(4)
N(3)–C(11)	1.52(4)	C(10)–O(1)	1.26(5)
C(8)–C(9)	1.31(6)	C(10)–C(11)	1.44(6)
N(1)–Au(1)–N(2)	82.8(11)	N(2)–Au(1)–N(3)	80.4(10)
N(3)–Au(1)–Cl(1)	97.4(9)	Cl(1)–Au(1)–N(1)	99.3(9)
C(8)–N(2)–C(10)	135(3)	O(1)–C(10)–C(11)	124(4)
C(8)–N(2)–Au(1)	109(2)	C(9)–N(1)–Au(1)	110(2)
Au(1)–N(1)–C(1)	127(3)	N(2)–C(8)–C(9)	121(4)
Au(1)–N(2)–C(10)	114(2)	N(2)–C(10)–C(11)	116(3)
C(11)–N(3)–Au(1)	110(2)		

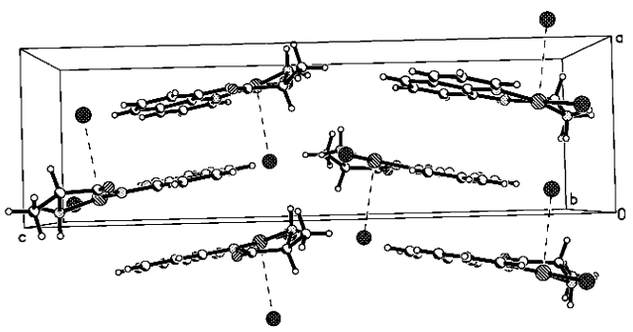

Fig. 4 Structure of complex **3** packed along the *a*-axis.

best plane being 0.1075 Å. The distance between the two adjacent planes is 3.2119 Å and π–π interactions also exist. The torsion angles Au(1)–N(2)–C(8)–C(9), Au(1)–N(1)–C(9)–C(8), Au(1)–N(2)–C(10)–C(11), Au(1)–N(3)–C(11)–C(10) are 4(3)°, −2.2(7)°, 2(5)° and −37(4)°, respectively. Different from that observed in complex **2**, the chloride counterion in complex **3** is not dissociated completely. The distance between Au(1) and Cl(2) is 3.308 Å, which suggests that a weak interaction may exist between them. There are intra- and inter-molecular hydrogen bonds observed in this complex, the D ··· A separations are 2.310 Å, 2.402 Å for N(3) ··· Cl(2a) and N(3) ··· Cl(2b) respectively (symmetry code: $x - 1/2$, $-y + 1/2$, $-z + 2$ and $x - 1$, y, z). The D–H ··· A angles are *ca.* 170.08° and 140.27° for N(3)–H(3B) ··· Cl(2a) and N(3)–H(3C) ··· Cl(2b), respectively.

In vitro antitumour activity

Fig. 5 shows the *in vitro* cytotoxic activities of complex **1** together with cisplatin against P388, HL-60, A-549 and BEL-7402 tumour cell lines. At a concentration of 10^{-5} mol L^{-1}, complex **1** showed an inhibition rate of over 40% against P388, HL-60 and A-549 tumour cell lines after 48 h. For A-549 cell line complex **1** demonstrated a strong inhibitory effect at a concentration of 10^{-6} mol L^{-1} which is about 3 times stronger than cisplatin, a clinically-used metal-containing antitumour drug.

The cytotoxic activities of complexes **2** and **3** against melanoma B16-BL6 cells are summarised in Fig. 6. Complex **3** exhibited higher activity than complex **2** at all the concentrations with an inhibition rate of 67.52% at a concentration of 10^{-7} mol L^{-1}.

UV-vis and fluorescence studies of DNA binding properties

The encouraging results from the preliminary cytotoxicity experiments prompted us to carry out DNA binding studies using UV and fluorescence spectroscopy.

Electronic absorption spectra. Before reacting complexes **1**–**3** with DNA, their solution behaviour in a mixed solution of 50% DMSO and 50% H_2O in the absence or presence of 50 mM

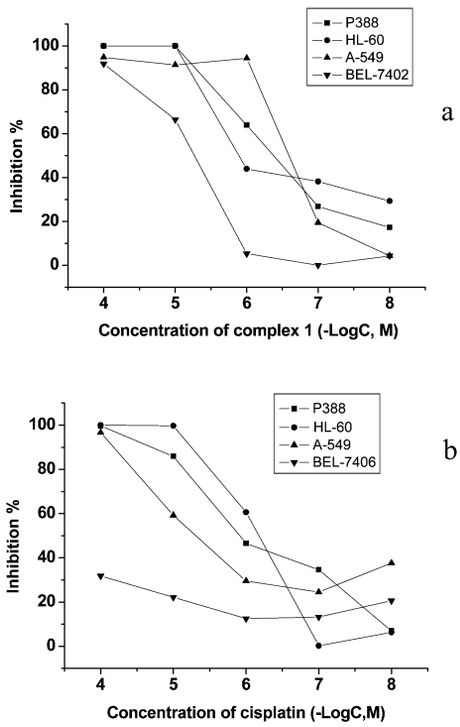

Fig. 5 Cytotoxic activity of complex **1** (a) and cisplatin (b) against selected tumour cell lines [-■- murine leukemia cells P-388, -•- human leukemia HL-60 cells, -▲- lung adenocarcinoma A-549 cells, -▼- human hepatoma BEL-7402 cells].

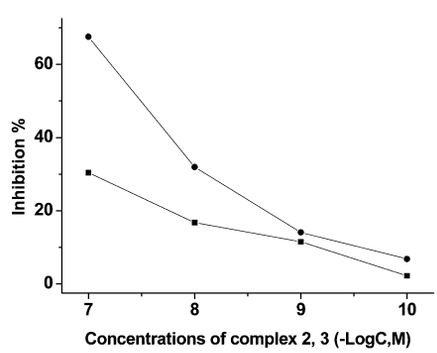

Fig. 6 Cytotoxic activity of complexes **2** (-■-) and **3** (-•-) against melanoma B16-BL6 cells.

NaCl was monitored by UV-vis spectroscopy for 24 h (Fig. S1 †). Only marginal spectral changes were observed in the absence of Cl^-, suggesting slow aquation occurs for these complexes. However, the aquation is completely inhibited by the presence of 50 mM Cl^-. These data suggest that the complexes are stable under the conditions studied.

The DNA binding experiment was conducted by reacting complexes **1**–**3** with CT-DNA at molar ratio $r = 0.1$. The UV spectra of the reaction recorded after 1–3 h are shown in Fig. 7. For complexes **1** and **3**, the intense LMCT transition band at around 360 nm assignable to a Cl⟶Au charge transfer transition decreased in intensity (hypochromism effect) with time after the addition of CT-DNA (Fig. 7b and Fig. S2 †). After three hours the absorption intensity dropped about 11% for complex **1** and 13% for complex **3**. The two shoulder bands between 305 and 330 nm disappeared gradually upon addition of DNA. The DNA binding of complexes **1** and **3** results in a blue shift (4–2 nm) of the UV band compared to that of the free complexes. These changes are not caused by the aquation process which is completely inhibited under these conditions (*vide supra*). They can not be explained by intercalative mechanisms either since a red shift would be expected due to the

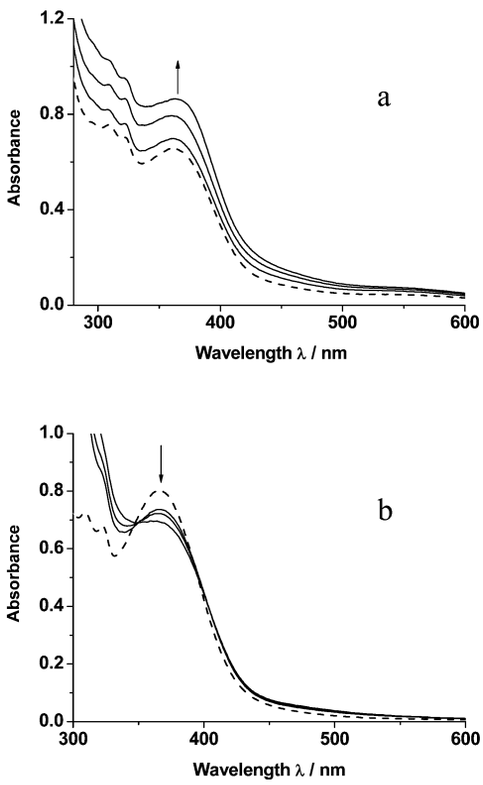

Fig. 7 UV absorption spectra of 2.1×10^{-4} mol L^{-1} complex **2** (a), 1.9×10^{-4} mol L^{-1} complex **3** (b) before (dashed line) and after (solid lines, represent 1 h, 2 h and 3 h, respectively) addition of calf thymus DNA at the ratio $r = 0.1$.

interaction between the aromatic chromophores and DNA base pairs.[27–29]

It is interesting to note that in contrast to that observed for complexes **1** and **3**, the UV band of complex **2** increased in intensity with a red shift of 4 nm after the addition of CT-DNA. This behaviour was previously observed for copper complexes,[30–32] and the hyperchromism was attributed to the dissociation of ligand aggregates and breakage of intermolecular hydrogen bonds when bound to DNA.

Fluorescence spectroscopic studies. The fluorescence emission spectra of EB bound to DNA in the absence and the presence of the three gold(III) complexes are shown in Fig. 8 and Fig. S3. † The emission band at 600 nm of the DNA-EB system decreased in intensity with an increase in the concentration of the three gold(III) complexes, which indicated that the complexes could replace EB from the DNA-EB system. Such a characteristic change is often observed in intercalative DNA interactions.[33]

Reactions with 5′-GMP

The interaction between the gold(III) complexes and model compound guanosine-5′-monophosphate (5′-GMP) were also investigated. The reaction mixture was examined by electrospray mass spectrometry (ESMS). For the reactions of complexes **1** and **2**, no Au(III)–GMP adduct was detected, which suggests that these two complexes can not bind to GMP covalently. For the reaction of complex **3**, apart from unreacted 5′-GMP a peak at 770.8 was observed which can be attributed to one negatively charged species $[(AuL_3)(GMP)]^-$ and another peak at 1133.7 to $\{[(AuL_3)(GMP)_2]^{2-} + H^+\}$. These data suggest that the Cl^- in complex **3** can be displaced by 5′-GMP, although the reaction extent is very limited.

The nature of the interactions between complexes **1**–**3** and calf thymus DNA can not be clarified unambiguously from the UV-vis, fluorescence and ESMS data. Since complexes **1**–**3** are all square planar and form a coplanar conformation with the quinoline ring such a molecular shape may facilitate intercalative binding towards DNA. The UV and fluorescence data support such a mechanism of reaction.

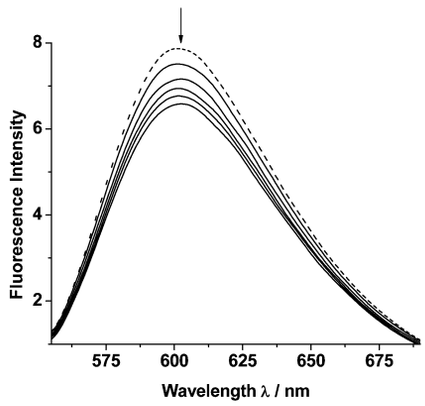

Fig. 8 Fluorescence emission spectra (excited at 526 nm) of the CT-DNA-EB system (4.905×10^{-5} mol L^{-1} EB, 4.905×10^{-5} mol L^{-1} DNA) in the absence (dashed line) and presence (solid line) of 2.4×10^{-4} mol L^{-1} complex **2** (20 μl per scan).

Conclusion

Taken together, the Au(III) complexes reported in this work have been fully characterized, and two of them have been examined by X-ray crystal diffraction. The Au(III) in these complexes shows a slightly distorted square planar coordination formed by three nitrogen atoms of the ligand and one chloride atom. All the complexes have shown considerable cytotoxic activity against several tumour cells, particularly notable for complex **1** against A-549 cell line and complex **3** against B16-BL6 cell line. The complexes are able to replace EB from the DNA-EB system, suggesting that they may intercalate into DNA. It is not clear whether such an interaction is responsible for the cytotoxicity observed.

References

1 B. Lippert (Editor), *Cisplatin: Chemistry and Biochemistry of a Leading Anticancer Drug*, Wiley-VCH, Weinheim, 1999.
2 P. J. Sadler and R. E. Sue, *Metal-based Drugs*, 1994, **1**, 107.
3 Z. J. Guo and P. J. Sadler, *Angew. Chem., Int. Ed.*, 1999, **38**, 1512.
4 Z. J. Guo and P. J. Sadler, *Adv. Inorg. Chem.*, 2000, **49**, 183.
5 C. F. Shaw III, *Chem. Rev.*, 1999, **99**, 2598.
6 C. K. Mirabelli, R. K. Johnson, C. M. Sung, L. F. Faucette, K. Muirhead and S. T. Crooke, *Cancer Res.*, 1985, **45**, 32.
7 S. T. Crooke and C. K. Mirabelli, *Am. J. Med.*, 1983, **75**, 109.
8 J. D. Bell, R. E. Norman and P. J. Sadler, *J. Inorg. Biochem.*, 1987, **31**, 241.
9 P. Calamai, S. Carotti, A. Guerri, L. Messori, E. Mini, P. Orioli and G. P. Speroni, *J. Inorg. Biochem.*, 1997, **66**, 103.
10 E. Bordignon, L. Cattalini, G. Natile and A. Scatturi, *J. Chem. Soc., Chem. Commun.*, 1973, 878.
11 J. Zou, Z. J. Guo, J. A. Parkinson, Y. Chen and P. J. Sadler, *Chem. Comm.*, 1999, 1359.
12 E. Kimura, Y. Kurogi and T. Takahashi, *Inorg. Chem.*, 1991, **30**, 4117; E. Kimura, Y. Kurogi, T. Koike, M. Shionoya and Y. J. Iitaka, *Coord. Chem.*, 1993, **28**, 33.
13 P. Calamai, A. Guerri, L. Messori, E. Mini, P. Orioli and G. P. Speroni, *Inorg. Chim. Acta*, 1999, **285**, 309.
14 F. Abbate, P. Orioli, B. Bruni, G. Marcon and L. Messori, *Inorg. Chim. Acta*, 2000, **311**, 1.
15 T. Yang, J. Y. Zhang, C. Tu, J. Lin, Q. Liu and Z. J. Guo, *Chin. J. Inorg. Chem.*, 2003, **19**, 45.
16 G. Marcon, S. Carotti, M. Coronnello, L. Messori, E. Mini, P. Orioli, T. Mazzei, M. A. Cinellu and G. Minghetti, *J. Med. Chem.*, 2002, **45**, 1672.
17 J. Y. Zhang, C. Tu, J. Lin, H. K. Fun, C. Suchad, X. Z. You and Z. J. Guo, *Chin. J. Inorg. Chem.*, 2002, **18**, 554.
18 J. Y. Zhang, X. K. Ke, C. Tu, J. Lin, J. Ding, L. P. Lin, H. K. Hun, X. You and Z. J. Guo, *Biometals*, 2003, **16**, 485.

19 J. Yergey, *Int. J. Mass Spectrom. Ion Phys.*, 1983, **52**, 337.
20 G. M. Sheldrick, *SAINT v4, Software Reference Manual*, Siemens Analytical X-ray Systems, Madison, WI, 1996.
21 G. M. Sheldrick, SADABS, Program for Emprical Absorption Correction of Area Detector Data, University of Gottingen, Germany, 1996.
22 G. M. Sheldrick, *SHELXTL v5, Reference Manual*, Siemens Analytical X-ray Systems, Madison, WI, 1996.
23 A. J. Wilson, *International Table for X-ray Crystallography*, Kluwer Academic Publishers, Dordrechet, 1992, vol. C, Tables 6.1.1.4 (p. 500) and 4.2.6.8 (p. 219), respectively.
24 M. C. Alley, D. A. Scudiero, A. Monks, M. L. Hursay, M. J. Czerwinski, D. Fine, B. J. Abbott, J. G. Mayo, R. H. Shoemaker and M. R. Boyd, *Cancer Res.*, 1988, **48**, 589.
25 P. Skehan, R. Storeng, D. Scudiero, A. Monks, J. McMahon, D. Vistica, J. T. Warren, H. Bokesch, S. Kenney and M. R. Boyd, *J. Natl. Cancer Inst.*, 1990, **82**, 1107.
26 L. Messori, F. Abbate, G. Marcon, P. Orioli, M. Fontani, E. Mini, T. Mazzei, S. Carotti, T. O'Connell and P. J. Zanello, *J. Med. Chem.*, 2000, **43**, 3541.
27 J. K. Barton, A. T. Danishefsky and J. M. Goldberg, *J. Am. Chem. Soc.*, 1984, **106**, 2172.
28 S. A. Tysoe, R. J. Morgan, A. D. Baker and T. C. Strekas, *J. Phys. Chem.*, 1993, **97**, 1707.
29 S. Satyanarayana, J. C. Dabrowiak and J. B. Chaires, *Biochemistry*, 1992, **31**, 9319.
30 F. Liu, K. A. Meadows and D. R. McMillin, *J. Am. Chem. Soc.*, 1993, **115**, 6699.
31 J. Liu, T. X. Zhang, T. B. Lu, L. H. Qu, H. Zhou, Q. L. Zhang and L. N. Ji, *J. Inorg. Biochem.*, 2002, **91**, 269.
32 M. Baldini, M. Belicchi-Ferrari, F. Bisceglie, G. Pelosi, S. Pinelli and P. Tarasconi, *Inorg. Chem.*, 2003, **42**, 2049.
33 C. V. Kumar, J. K. Barton and N. J. Turro, *J. Am. Chem. Soc*, 1985, **107**, 5518.